ATPase Kinetic Characterization and Single Molecule Behavior of Mutant Human Kinesin Motors Defective in Microtubule−Based Motility †

ARTICLE *in* BIOCHEMISTRY · JUNE 2000

Impact Factor: 3.02 · DOI: 10.1021/bi9928344 · Source: PubMed

4 AUTHORS, INCLUDING:

Kurt S Thorn
University of California, San Francisco
32 PUBLICATIONS **3,711** CITATIONS

SEE PROFILE

ATPase Kinetic Characterization and Single Molecule Behavior of Mutant Human Kinesin Motors Defective in Microtubule-Based Motility†

Takashi Shimizu,‡,§ Kurt S. Thorn,§,|| Aaron Ruby,§ and Ronald D. Vale*,§,⊥

National Institute of Bioscience and Human-Technology and National Institute for Advanced Interdisciplinary Research, Higashi, Tsukuba, Ibaraqi 305, Japan, Department of Cellular and Molecular Pharmacology, Graduate Group in Biophysics, University of California, San Francisco, California 94143, and Howard Hughes Medical Institute, San Francisco, California 94143

Received December 9, 1999; Revised Manuscript Received February 28, 2000

ABSTRACT: Conventional kinesin is a microtubule-based motor protein that is an important model system for understanding mechanochemical transduction. To identify regions of the kinesin protein that participate in microtubule binding and force production, Woehlke et al. [(1997) *Cell 90*, 207−216] generated 35 alanine mutations in solvent-exposed residues. Here, we have performed presteady-state kinetic and single molecule motility analyses on three of these mutants [Y138A, loop 11 triple (L248A/D249A/E250A), and E311A] that exhibited a similar ∼3-fold reduction in both microtubule gliding velocity and microtubule-stimulated ATPase activity. All mutants showed normal second-order ATP binding kinetics, indicating correct folding of the active site. The Y138A and loop 11 triple mutants were defective both in nucleotide hydrolysis and in microtubule-stimulated ADP release rates, the latter suggesting a defect in allosteric communication between the microtubule and the active site. A single molecule fluorescence assay further revealed that the loop 11 mutant is defective in initiating processive motion, suggesting that this loop is important for the initial contact between kinesin and the microtubule. Y138A, on the other hand, can bind to the microtubule normally but cannot move processively. For E311A, neither the rate of nucleotide hydrolysis nor ADP release could account for its slower ATPase and gliding velocity, which suggests that either phosphate release or a conformational transition is rate-limiting in this mutant. The single molecule assay showed that E311A has a reduced velocity of movement, but is not defective in processivity. Thus, while these mutants behave similarly in solution ATPase and multiple motor gliding assays, kinetic and single molecule analyses reveal defects in distinct processes in kinesin's mechanochemical cycle.

Conventional kinesin is a molecular motor that is thought to transport membrane organelles (*1*) and intermediate filaments (*2*, *3*) along microtubules. In higher eukaryotes, conventional kinesin is composed of two heavy chains (∼120 kDa) and two light chains (60−80 kDa)(*4*). The N-terminal 340 amino acid residues of the heavy chain form a globular domain, which contains the microtubule and ATP binding sites. This domain operates as a plus end-directed microtubule motor in the absence of the remainder of the heavy chain polypeptide as well as the light chains (*5*). Beyond this motor domain, there is an extended coiled-coil region that facilitates dimerization and contains conserved sequences at its C-terminus for light chain binding (*4*). The C-terminal ∼100 residues of the kinesin heavy chain comprise a small globular domain that, together with the light chains, may mediate attachment to intracellular cargo.

In recent years, conventional kinesin has been extensively studied as a model system for understanding chemomechanical transduction. Single molecule motility studies have shown that kinesin can move along a single protofilament (*6*) in steps of 8 nm (the size of the tubulin dimer) each time that it hydrolyzes an ATP (*7*, *8*). Unlike many other molecular motors, such as muscle myosin, conventional kinesin is a highly processive motor and can take >100 steps along a microtubule before dissociating from the filament (*9*). A considerable effort has been devoted to defining the rate constants that govern the intrinsic and microtubule-stimulated ATPase cycles of conventional kinesin (*10*−*13*). Both the hydrolysis step (*14*) and the ADP dissociation step (*15*) are accelerated by microtubules (10- and 1000-fold, respectively). The microtubule dissociation step (*14*, *16*) occurs after hydrolysis of the $\beta-\gamma$-pyrophosphate bond, although the exact timing of this event in the cycle is still poorly defined.

Understanding the structural basis of kinesin motility has been aided by determination of crystal structures for the motor domains of human (*17*) and rat (*18*, *19*) kinesin as

† T.S. and K.S.T. equally contributed to this work. This work was supported, in part, by grants-in-aid from the Agency of Industrial Science and Technology, M.I.T.I. (T.S.), and by a program project grant from the National Institutes of Health (R.D.V.). K.S.T. is supported by an HHMI predoctoral fellowship.

* Correspondence should be addressed to this author at the Department of Cellular and Molecular Pharmacology, Box 0450, 513 Parnassus Ave., University of California, San Francisco, San Francisco, CA 94143. Tel: (415) 476-6380. FAX: (415) 476-5233. E-mail: vale@phy.ucsf.edu.

‡ National Institute of Bioscience and Human-Technology.

§ Department of Cellular and Molecular Pharmacology, University of California, San Francisco.

|| Graduate Group in Biophysics, University of California, San Francisco.

⊥ Howard Hughes Medical Institute.

10.1021/bi9928344 CCC: $19.00
Published on Web 04/13/2000

well as of *Drosophila* ncd (*20, 21*) and yeast kar3 (*22*), two minus end-directed motors of the kinesin superfamily. These structures revealed that the core secondary structural elements of the kinesin motor domain show a surprising homology to the catalytic domain of both the actin-based motor myosin and G proteins, a superfamily of molecular switches. These observations suggest that motors and molecular switches evolved from a common ancestor (*23*) and may share similar strategies for nucleotide-dependent conformational changes during their enzymatic cycles (*24*).

The availability of a kinesin motor domain structure also provided an opportunity to define regions that are involved in microtubule binding, nucleotide hydrolysis, and mechanochemical transduction. In a recent study aimed at identifying residues that interact with microtubules, Woehlke et al. (*25*) mutated 35 solvent-exposed residues to alanine on one face of the kinesin motor domain and then examined the effects on microtubule-stimulated ATPase and in vitro motility activities. This study indicated that the microtubule interface is extensive, although the most important residues are clustered at or near the L12/α5 region. A triple mutant in this region, for example, displayed very little microtubule binding, even in the presence of AMPPNP,[1] which normally induces a tight binding state in kinesin. While 14 mutations were identified that altered microtubule affinity by 2-fold or greater, only 2 of the 35 single point mutations substantially decreased motility and ATPase k_{cat} (Y138A and E311A). In addition, a triple mutant in L11 [also known as the switch II loop, since it contains residues that are thought to be involved in sensing release of the γ-phosphate (*21*)] and the L12 triple mutant exhibited significant defects in microtubule gliding and ATPase turnover.

These four mutations that showed decreased microtubule-stimulated ATPase and microtubule-translocating activities could provide insight into how different regions on the surface of kinesin motor domain participate in the enzymatic pathway that leads to force production. In this study, we have carried out kinetic investigations to identify the underlying enzymatic steps that are defective in these mutant kinesin motors and also examined how these mutants interact with microtubules at the single molecule level.

EXPERIMENTAL PROCEDURES

Chemicals. MantATP, a gift from Dr. Edwin Taylor (University of Chicago), was synthesized by the method of Hiratsuka (*26*) but was purified by DEAE-Sephadex A-25 column chromatography with a triethylammonium bicarbonate gradient, instead of the original Sephadex LH20 chromatography. [γ-^{32}P]ATP (PB 170) was from Amersham, Inc. Other reagents were of analytical grade. The ingredients of the solutions used in this study were 25 mM Pipes−NaOH (pH 6.8), 50 or 200 mM NaCl, 2 mM $MgCl_2$, 0.5 mM EGTA, 0.5 mM DTT, and 2.5% sucrose, unless described otherwise.

Preparation of Kinesin Proteins. The wild type and mutants used in this study consisted of amino acids 1−420 of human ubiquitous kinesin heavy chain (K420). In short, BL21 cells were freshly transformed with the K420 construct, inoculated into TPM (20 g of bacto-tryptone, 15 g of bacto-yeast extract, 8 g of NaCl, 2 g of glucose, 2 g of Na_2HPO_4, and 1 g of KH_2PO_4 in 1 L of H_2O at pH 7) medium, and grown at 37 °C until the A_{600} reached 0.8−1.2. Expression was then induced with 0.2 mM IPTG at 25 °C for 12−16 h. The cells were broken with a Small Volume Microfluidizer M-110S (Microfluidics Corp., Newton MA) in extract buffer: 25 mM Pipes−KOH (pH 6.8), 2 mM $MgCl_2$, 1 mM EGTA, 0.5 mM DTT, and 1 mM Pefabloc (Boehringer Mannheim, Inc.). A high-speed supernatant of *E. coli* extract was prepared and was applied to a P-cellulose column (10−12 mL bed per liter of culture) equilibrated in extract buffer containing 0.1 M KCl. A 0.1−1 M KCl gradient was then applied to the column, and K420 or a mutant was eluted around 0.4 M KCl. The pooled fraction was then diluted to 0.15 M KCl and applied to a 5 mL HiTrap SP column equilibrated in 0.15 M KCl in extract buffer. The K420-containing flow-through was then further diluted to 0.1 M KCl in extract buffer and applied to a MonoQ column equilibrated in the same buffer. A 40 mL 0.1−0.5 M KCl gradient was applied to the column, and the K420 peak eluted at 0.25 M KCl. The peak fractions were pooled, 25 μM ATP and 10% sucrose were added, and aliquots were stored in liquid N_2. Typically, 8−20 mg of >85% pure protein could be obtained per liter of culture.

K560GFP constructs were prepared essentially as described *(27)* except that a REsource Q15 column was used for the anion exchange step. All K560GFP constructs were further purified by microtubule affinity *(27)* before assaying. After the microtubule affinity purification, motors were either assayed immediately or frozen with 15% sucrose added and stored in liquid nitrogen until assaying.

Quantitation of protein concentration was performed as described previously (*25*).

Stopped-Flow Assay. Stopped-flow assays were carried out with a Kintek SF2001 stopped-flow apparatus at 22 °C. MantATP or mantADP was excited at 350 nm, and the fluorescence was monitored at 90° through a 410 nm cutoff filter. The emission maximum was at 450 nm. Due to higher background fluorescence at high mantATP concentrations, the signal-to-noise ratio did not permit accurate measurements above 0.05 mM mantATP with 0.01 mM enzyme active site.

Quench-Flow Assay. K420, or its mutant, was incubated with 0.5 M NaCl and 4 mM EDTA to strip the bound MgADP, and then gel-filtrated at 22 °C through a prepacked gel exclusion column (10 DG, BioRad) equilibrated with a solution consisting of 25 mM Pipes−NaOH (pH 6.8), 0.4 M NaCl, 2 mM EDTA, 0.5 mM DTT, and 5% sucrose. The resultant protein, placed on ice immediately, was essentially nucleotide-free, as judged by UV absorption spectra of its acid supernatant (5% nucleotide remaining at most).

The thus obtained nucleotide-free K420 was made 4 mM in $MgCl_2$ and then diluted with an equal volume of the buffer solution above, except that 15% sucrose and no NaCl were present. The final solution contained 30 μM protein (enzyme active sites), 25 mM Pipes−NaOH (pH 6.8), 0.2 M NaCl, 4 mM $MgCl_2$, 2 mM EDTA, 0.5 mM DTT, and 10% sucrose. This mixture was loaded into a quench-flow sample loop of a Kintek RQF-3 quench-flow apparatus (Kintek, Inc.). The

[1] Abbreviations: mantADP, 2′(3′)-*O*-(*N*-methylanthraniloyl)adenosine 5′-diphosphate; mantATP, 2′(3′)-*O*-(*N*-methylanthraniloyl)adenosine 5′-triphosphate; IPTG, isopropyl β-D-thiogalactoside; GFP, green fluorescent protein; AMPPNP, adenylyl imidodiphosphate; DTT, dithiothreitol; EGTA, ethylene glycol bis(β-aminoethyl ether)-*N*,*N*,*N*′,*N*′-tetraacetic acid; Pipes, piperazine-*N*,*N*′-bis(2-ethanesulfonic acid).

other sample loop was loaded with a radioactive ATP solution in the same buffer solution. After mixing 1 to 1 in the quench-flow apparatus, the protein and ATP concentrations were 15 and 50 μM, respectively. This enzyme−ATP mixture was allowed to incubate for a designated amount of time, usually from 5 to 1000 ms, and was then mixed with final 1 M HCl and 1 mM carrier inorganic phosphate in order to quench the enzyme reaction. The quench-flow apparatus was operated in the "constant volume mode", where the quenched solution out of the apparatus was designed to have constant volumes. To separate nucleotide from the released [^{32}P]phosphate, the solution was centrifuged to pellet the denatured protein, mixed with a charcoal suspension (final 0.05 g/mL), and centrifuged again to pellet the charcoal. An aliquot of supernatant was transferred into a scintillation vial containing 2 mL of H_2O. The radioactivity was measured by Cerenkov counting.

In the case of the quench-flow experiments with K420−microtubule complex, microtubules without free GTP (obtained by centrifugation through a 40% sucrose cushion in nucleotide-free buffer containing 20 μM taxol) were mixed with K420 at room temperature. The buffer solution ingredients were 25 mM Pipes−NaOH (pH 6.8), 50 mM NaCl, 2 mM $MgCl_2$, 0.5 mM EDTA, 0.5 mM DTT, and 2.5% sucrose. A K420−microtubule suspension [50 μM microtubules (tubulin dimer concentration) and 30 μM K420 (active site concentration)] was left standing for 20 min, and then loaded into the quench-flow apparatus. The concentrations after mixing in the apparatus were 25 μM microtubules, 15 μM K420 enzyme active site, and 100 μM ATP. The rest of the procedure was the same as above for nucleotide-free K420 or a mutant. The ADP bound at the active site of kinesin was not removed, so that some nucleotide in this dimeric motor likely remained at the active site even after the microtubule incubation. This probably decreased the burst size, although the burst kinetics should not have been affected.

Single Molecule Fluorescence Measurements. Single molecule motility measurements were performed essentially as described *(28)*, except that 0.5 mg/mL casein was used as the blocking protein instead of 7.5 mg/mL bovine serum albumin. All measurements were performed at 5 mW incident power. Data were recorded on sVHS videotape with four-frame averaging and analyzed off-line using a custom set of macros in NIH-IMAGE. Segments of videotape were digitized at 10−15 fps, and the outline of the axoneme (determined from the Cy5 image) was superimposed on the GFP signal. Attachment and detachment times and positions were determined manually and recorded for each spot interacting with the axoneme. These were then converted to run length, association time, and velocity. Run lengths and association times were then determined by nonlinear least-squares fitting of the cumulative probability distribution from x_0 to infinity to $1 - \exp[(x_0 - x)/t]$. The lower threshold, x_0, is used to exclude short runs which are undersampled and was chosen for each data set by manual examination of the run length histogram. For wild-type K560GFP, x_0 was chosen to be 0.5 μm. For fitting association times, x_0 was derived from the x_0 used to fit run lengths by dividing by the measured velocity. Velocities were determined by fitting the cumulative probability distribution to the Gaussian cumulative probability distribution. All fitting was performed in MATLAB. Errors were estimated by the bootstrap technique *(29)*. Each distribution was resampled 200 times and fit as described above. The standard deviation of the fitted parameter over the resampled data sets was taken as the error in the fitted quantity. The photobleaching rate was taken as the rate of disappearance of GFP-kinesin nonspecifically adsorbed to the slide and was 0.08 s^{-1}.

Table 1: Enzymological and Motile Characteristics of K560 and Three Alanine Mutants[a]

	MT-stimulated ATPase		
mutation	K_mMT (mM)	k_{cat} (s^{-1})	MT gliding (μm/s)
wild type	1.1 ± 0.35	27 ± 7	0.53 ± 0.10
Y138A	0.97 ± 0.22	9.5 ± 1.1	0.12 ± 0.03
E311A	0.35 ± 0.01	9.2 ± 1.6	0.16 ± 0.07
L11 triple	1.1 ± 0.40	5.7 ± 1.1	0.14 ± 0.03

[a] The data are taken from Woehlke et al. (*25*). K_mMT and k_{cat} indicate the microtubule concentration needed for half-maximal stimulation of the ATPase activity and the maximal ATPase activity at saturating microtubule concentrations.

RESULTS

In our previous study (*25*), the human kinesin heavy chain fragment from amino acid residues 1−560 (K560) was used for analyzing mutations. However, since this protein cannot be easily purified to high yield for kinetic studies, we prepared wild-type and mutant proteins in the dimeric construct K420 (J. Kull, unpublished results), which expresses much larger quantities of soluble protein. In this study of wild-type and mutant K420 motors, we analyzed rates of nucleotide binding, nucleotide hydrolysis in the absence and presence of microtubules, and ADP dissociation in the absence and presence of microtubules.

The steady-state ATPase and motility phenotypes of these mutants from the previous study (*25*) are summarized in Table 1. The locations of the mutated, solvent-exposed residues that were examined in this study are shown in Figure 1. Y138A is a mutation in superfamily conserved residue in L7, which is located close to the switch I region in the γ-phosphate region of the nucleotide. The triple mutant L248A/D249A/E250A (L248 and E250 are superfamily conserved) is located at the tip of L11 (herein referred to as L11 triple). The base of L11 contains residues that may hydrogen bond with the nucleotide γ-phosphate (*21*); the tip of L11 may also contact the microtubule (*30*). The triple mutant Y274A/R278A/K281A (all residues are superfamily conserved) is found in L12 (herein referred to as L12 triple), which was proposed to function as the principle microtubule binding region of kinesin (*25*). E311A is a mutation in a superfamily conserved residue in α6, a helix that may connect the catalytic core to a mechanical amplifier region (the neck linker) (*27, 31*).

MantATP Binding to Nucleotide-Free K420s. The rate of ATP binding to nucleotide-free wild-type or mutant K420 was investigated using a fluorescent ATP analogue, mantATP, whose fluorescence increases when bound to the enzyme active site. As reported by Ma and Taylor (*10, 32*), the signal of the wild-type K420 was biphasic and could be fitted with two exponentials (Figure 2). The rate of the first phase increased with increasing mantATP concentration, reflecting the second-order reaction kinetics for nucleotide

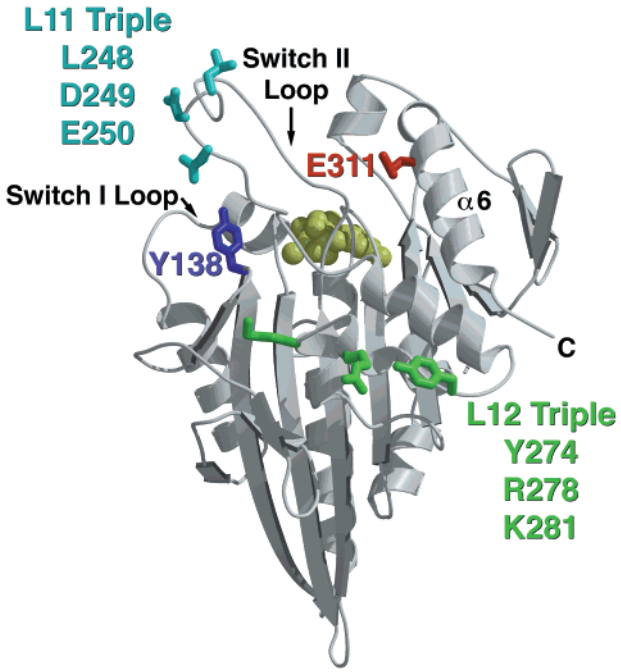

FIGURE 1: Three-dimensional structure of human kinesin catalytic core. The figure has been constructed after the coordinates by Kull et al. *(17)*. The residues that have been mutated are highlighted. The bound ADP is drawn with yellow−green shade. Note that all residues of the present study are not in direct vicinity of the bound ADP.

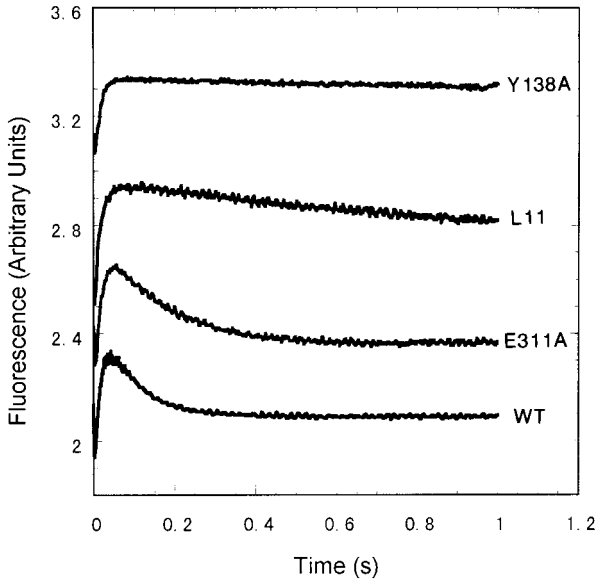

FIGURE 2: MantATP binding to the ADP-free K420 or a mutant monitored by fluorescence stopped-flow method. Stopped-flow fluorescence traces are shown. The ADP-free K420, wild type or a mutant, was mixed with mantATP in the stopped-flow apparatus. The final concentrations after mixing were 8 μM enzyme active site and 20 μM mantATP, respectively, and the solution ingredients were 25 mM Pipes−NaOH (pH 6.8), 0.2 M NaCl, 4 mM $MgCl_2$, 2 mM EDTA, 0.5 mM DTT, and 10% sucrose. The temperature was 22 °C. Traces of wild-type (WT), E311A, and L11 triple mutants could be fitted with double exponentials (rising phase and the falling phase), and the rates were 68 and 15 s^{-1} for wild type, 54 and 6 s^{-1} for E311A mutant, and 62 and 0.6 s^{-1} for L11 triple mutant, respectively. The trace of Y138A mutant could be fitted with a single exponential (rising phase only), and the rate was 72 s^{-1}.

binding (Figure 3). The smaller and decreasing second phase was independent of the mantATP concentration (*10*).

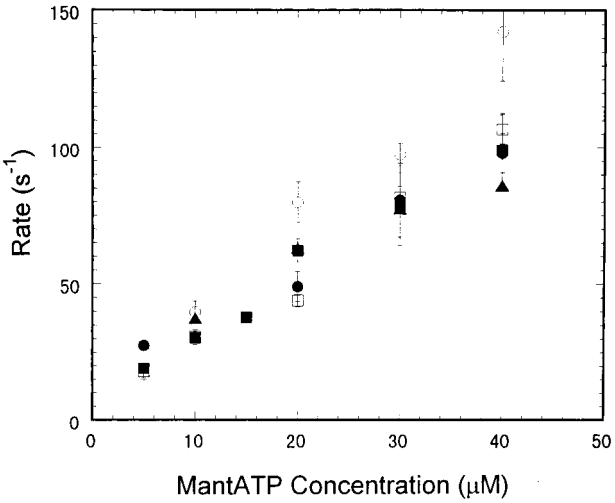

FIGURE 3: Dependence of fluorescence change rates on mantATP concentration. The rate of the rising phase of the fluorescence upon mixing of ADP-free K420 or a mutant with mantATP (see Figure 2) was estimated and plotted against the mantATP concentrations. ●, ■, ▲, ○, and □ indicate the data with the wild type, E311A, L11 triple, Y138A, and L12 triple mutant, respectively. Error bars indicate standard deviations. From the slope, the second-order rate constants could be estimated to be 2.2 × 10^6, 2.3 × 10^6, 1.6 × 10^6, 3.4 × 10^6, and 2.6 × 10^6 M^{-1} s^{-1}, respectively. The falling phase such as seen in Figure 2 did not show a dependence on mantATP concentration.

For mantATP binding, wild-type K420 and the mutants showed similar second-order rate constants (Table 2). The Y138A mutant even exhibited somewhat higher rates. In contrast, the second, decreasing fluorescence phase was affected in several mutants. This phase in wild-type kinesin occurred at a rate of 15 ± 4 s^{-1}; the L12 triple mutant exhibited a similar rate. However, the E311A mutant exhibited a ∼2-fold slower rate (6.0 ± 0.6 s^{-1}), and the L11 triple mutant displayed an even slower rate (0.6 ± 0.08 s^{-1}). Strikingly, the Y138A mutant did not show an observable second phase. According to Ma and Taylor (*10*, *32*), the decreasing phase of mantATP fluorescence may be related to the ATP hydrolysis step. An alternative explanation for this decreasing phase is the isomerization of mantADP isomers; however, the rate constant for this process is 2 orders of magnitude slower than that observed here (*33*). To establish whether the E311A, L11 triple, and Y138A mutants were indeed compromised in ATP hydrolysis, we next measured the initial burst of phosphate production, as described below.

ATP Hydrolysis Assayed by the Quench-Flow Method. Before measuring the rate of ATP hydrolysis using a quench-flow apparatus, we first examined whether K420 or a mutant, which had been treated with EDTA to remove the bound ADP, exhibited a phosphate burst by the manual quenching method (0−20 s). Wild-type kinesin exhibits a phosphate burst because ATP hydrolysis is not rate limiting in the kinetic cycle. The ADP-free wild-type K420 as well as the L11 triple, L12 triple, and E311A mutants all exhibited a phosphate burst of ca. 0.4 mol of phosphate/mol of motor domain, which is consistent with the previously reported values (*32*, *34*, *35*). In contrast, the Y138A mutant showed very little, if any, burst of phosphate production.

With a quench-flow apparatus, we next investigated the transient phase of the phosphate burst. As shown in Figure

Table 2: ATPase Kinetic Parameters of K420 Wild Type and Mutants[a]

	mantATP binding		rate of phosphate burst (s^{-1})		mantADP dissociation		
mutant	on rate ($M^{-1}\,s^{-1}$)	decreasing phase rate (s^{-1})	−MT	+MT	basal rate (s^{-1})	maximal rate (s^{-1})	half-maximal MT (μM)
wild type	2.2×10^6	15	17	60	0.016	70	34
Y138A	2.3×10^6	no phase	no burst	no burst	0.033	37	81
E311A	1.6×10^6	6	3.6	14	0.080	89	16
L11 triple	3.4×10^6	0.6	0.31	2.6	0.016	8.5	5
L12 triple	2.6×10^6	15	nd	nd	0.025	**a**	**a**

[a] Summary of the rates and rate constants of the ATPase of K420 wild type and mutants. For experimental conditions, see the appropriate figure legend and Experimental Procedures. MT indicates microtubules. **a** in the table means that those experiments were not done since the L12 triple mutant exhibits extremely poor binding to the microtubules. nd, not determined.

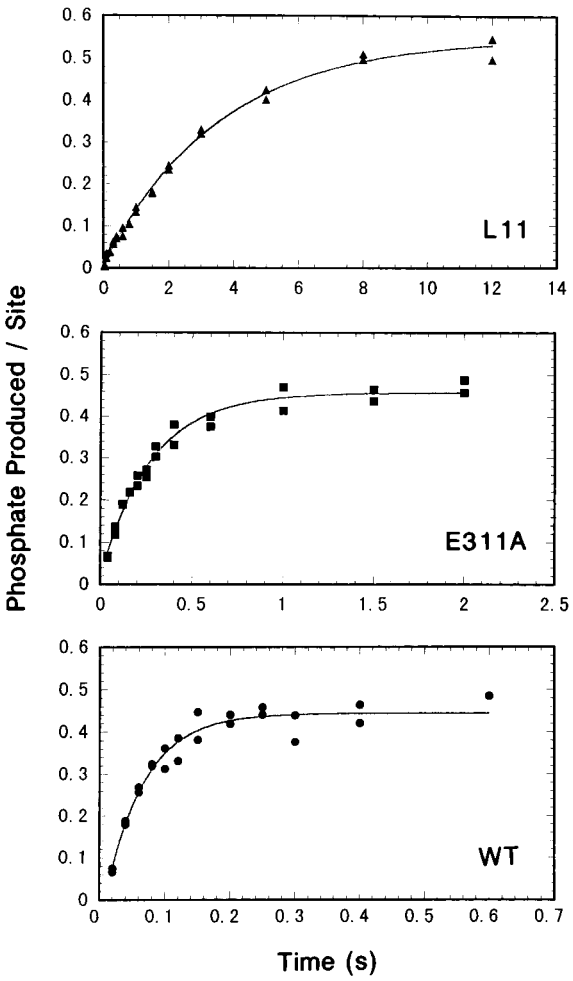

FIGURE 4: Initial burst of phosphate production by K420 or a mutant in the absence of microtubules. Final 15 μM ADP-free K420 wild type or mutant (expressed as enzyme active site), indicated in the figure, was mixed with 50 μM radioactive ATP in the quench-flow apparatus and allowed to perform the ATP turnover reaction for a designated duration of time as indicated on the abscissa. The solution ingredients were the same as those described in the legend to Figure 2. The temperature was 22 °C. The lines are the fits with an exponential phase and a subsequent slow steady-state phase. From the exponential phase, we estimate the hydrolysis step rate to be 17, 3.6, and 0.31 s^{-1} for the wild type, E311A, and L11 triple mutant, respectively.

4, the wild-type K420 showed a phosphate burst rate of ca. 17 s^{-1}. The E311A mutant displayed a slower burst rate (3.6 s^{-1}), while the L11 mutant exhibited a much slower burst phase (0.31 s^{-1}). These relative rates are similar to those measured for the decreasing phase of the mantATP fluorescence as described above.

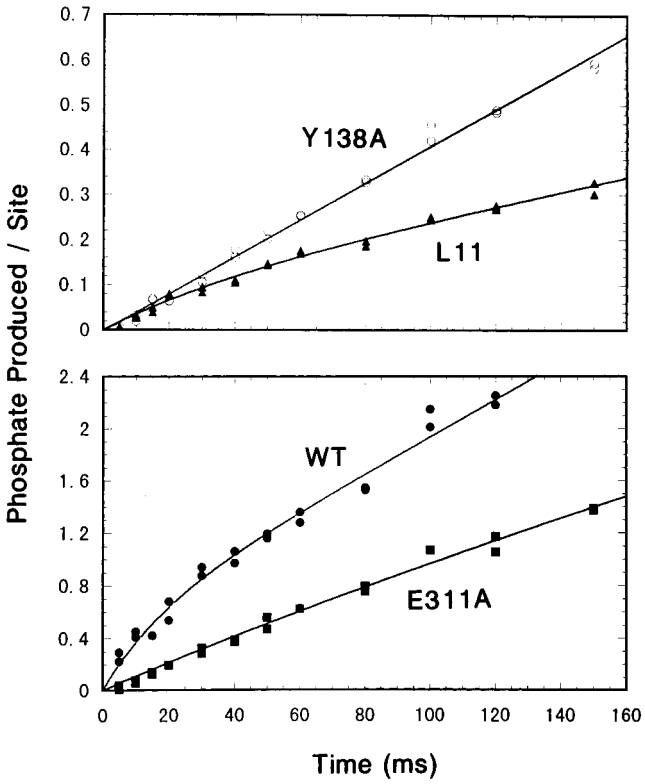

FIGURE 5: Initial burst of phosphate production by K420 or a mutant in the presence of microtubules. K420, wild type or mutant, complexed with microtubules was mixed with radioactive ATP in the quench-flow apparatus. Final concentrations of the enzyme active site, microtubules (tubulin dimer concentration), and ATP were 15 μM, 25 μM, and 0.1 mM, respectively. The solution ingredients were 25 mM Pipes−NaOH (pH 6.8), 50 mM NaCl, 2 mM $MgCl_2$, 0.5 mM EGTA, and 2.5% sucrose. The wild-type K420 exhibited an obvious phosphate burst, while E311A and L11 triple mutant showed small bursts; 0.48, 0.13, and 0.086 phosphate per active site, respectively. On the other hand, Y138A mutant did not show the burst phase. The steady-state rates were 14.2, 8.6, 1.6, and 4.1 s^{-1} for the wild-type, E311A, L11 triple, and Y138A mutant, respectively. Those numbers are smaller than the k_{cat}s due to the nonsaturating microtubule concentration. The nonsaturating microtubule concentration also results in a smaller activation of ATP hydrolysis than previously observed.

We also investigated the phosphate burst rate of K420 complexed with microtubules. The burst size of the wild type was around 0.4/mol of enzyme site, probably because the microtubules did not displace all of the ADP in the kinesin active site (Figure 5)(*11, 13, 14, 36*). Although the rates of the transient phase were difficult to estimate, wild type, E311A, and L11 triple mutants exhibited burst kinetics, the burst sizes being much smaller with the E311A and L11

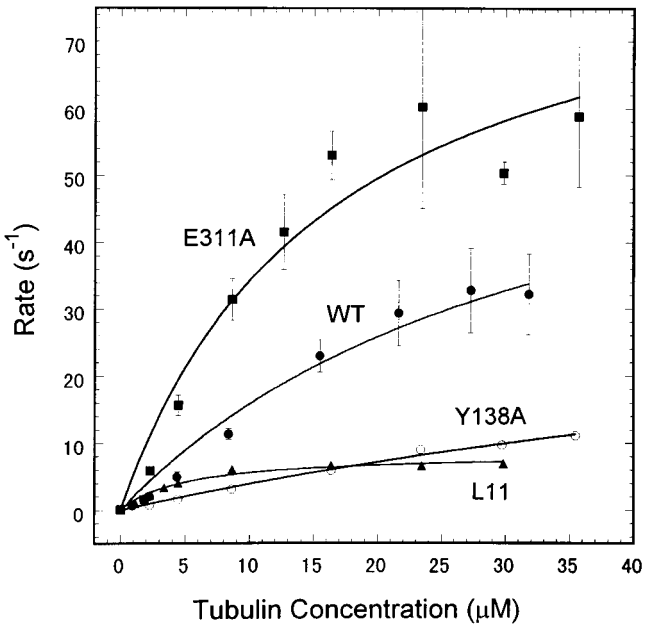

FIGURE 6: Dissociation of mantADP from K420 wild type or a mutant, and its acceleration by microtubules. The K420 wild type or a mutant having mantADP at the active site was prepared as described under Experimental Procedures. The enzyme in buffer solution containing 25 mM Pipes−NaOH (pH 6.8), 50 mM NaCl, 2 mM $MgCl_2$, 0.5 mM EGTA, and 2.5% sucrose was mixed with a large excess of ATP with or without microtubules in the stopped-flow apparatus. The final concentrations of the enzyme active site and ATP were 2−4 μM and 0.5 mM, respectively, and that of microtubules expressed as tubulin dimer concentration is indicated on the abscissa. The excitation was at 350 nm, and the emission was monitored through a 410 nm long-pass filter. The stopped-flow traces were fitted with single exponentials, and the rates estimated are plotted against the microtubule concentration. The lines are the fits to hyperbolae. The maximal rates at infinite microtubule concentration and the microtubule concentrations giving half-maximal acceleration were estimated to be 70 s^{-1} and 34 μM for the wild type, 89 s^{-1} and 16 μM for E311A, 8.5 s^{-1} and 5 μM for L11 triple, and 37 s^{-1} and 81 μM for Y138A, respectively. Error bars indicate the standard deviations.

triple mutants. On the other hand, the Y138A mutant displayed little, if any, phosphate burst upon ATP addition to the microtubule−K420 complex.

MantADP Dissociation and Its Acceleration by Microtubules. The dissociation of mantADP from wild-type or mutant K420 after mixing with a large excess of ATP was investigated in the absence and presence of microtubules. In the absence of microtubules, the wild-type K420 displayed a slow mantADP dissociation rate (0.016 s^{-1}). The mutants exhibited similar rates, with the exception of E311A which released mantADP at a faster rate (0.08 s^{-1}).

Upon addition of microtubules, the release of mantADP is dramatically accelerated. In the presence of microtubules and ATP, ADP release from the two heads of kinesin dimers occurs sequentially. ADP is released from one head on binding to the microtubule, and binding of ATP to this head enables release of ADP from the second head (*11*). Since we cannot resolve these two steps in this experiment, we measured an apparent rate constant for ADP release corresponding to the average of the two sequential steps (*10, 32*). As seen in Figure 6, the dissociation rates varied considerably among the wild-type and mutant K420 proteins. At 9 μM microtubules, the rate of wild-type K420 was 11.4 ± 0.8 s^{-1}, which is consistent with previously observed values at this microtubule concentration (*14, 37*). In sharp contrast, the L12 triple mutant did not accelerate its release of mantADP, even in the presence of microtubules. This result is consistent with previous findings showing that the L12 mutant binds poorly to the microtubules, even in the presence of AMPPNP (*25*). At the same microtubule concentration, the dissociation rates of mantADP from the L11 triple (6.1 ± 0.2 s^{-1}) and Y138A (3.1 ± 0.1 s^{-1}) mutants were 2- and 4-fold slower than wild-type K420, respectively. On the other hand, the E311A mutant released mantADP in the presence of a similar concentration of microtubules at 3-fold higher rates (31.5 ± 3 s^{-1}) compared with wild type (Figure 6), even though the k_{cat} of E311A was about one-third of the wild type (see Discussion).

Table 3: Single Molecule Motility of Kinesin Mutants[a]

		run length (μm)			
construct	N	observed	corrected	T_{on} (s)	velocity (μm/s)
WT	246	1.4 ± 0.1	2.0 ± 0.3	3.7 ± 0.2	0.398 ± 0.004
E311A	110	0.8 ± 0.1	1.3 ± 0.3	4.6 ± 0.6	0.184 ± 0.008
L11 triple	25	0.6 ± 0.2	≥1.7	11.0 ± 3	0.073 ± 0.01
Y138A	114	−	−	2.0 ± 0.3	<0.07

[a] Single molecule measurements were made as described under Experimental Procedures. N is the number of events that were scored for each mutant. Run lengths, association times (T_{on}), and velocities were fit to the observed data as described under Experimental Procedures. Errors were determined by bootstrapping and are reported as one standard deviation. All measurements were repeated on two separate preparations and agreed within error. The numbers reported here are derived from a single fit of all measured data. Run lengths were corrected for photobleaching using the following formula: $RL_{corr} = RL_{meas} * k_{off}/(k_{off} - k_{bleach})$, where $k_{off} = 1/T_{on}$ and k_{bleach} was determined to be 0.08 s^{-1} by measuring the disappearance rate of spots nonspecifically adsorbed to the glass. The run length correction for L11 is uncertain, as $k_{off} \approx k_{bleach}$, and only a lower bound on the run length could be determined Because no motility was detected for any Y138A spots, including the 10% that remained associated with the axoneme for more than 3 s, an upper bound for the Y138A velocity was derived assuming that runs longer than 0.2 μm are detectable.

Single Molecule Behavior of Mutant Kinesins. To understand in greater detail how these mutations affect the motility of kinesin, we examined these mutants in a single molecule fluorescence motility assay (Table 3). In this assay, the motion of a single GFP-tagged kinesin is followed as it moves along an axoneme. From these measurements, we can determine the velocity, the distance traveled per encounter with the axoneme (the run length), and the frequency of motility events. The run length is a measure of the cooperativity between kinesin heads necessary for processive motion, and the frequency of motility events is a measure of the ability of the kinesin to initiate processive motion. To perform these measurements, the mutants were subcloned into a dimeric K560GFP construct, which has been extensively characterized in this assay *(38)*. We chose not to study the L12 triple mutant because of its low affinity for microtubules.

The E311A mutant was motile in the single molecule motility assay. The frequency of motility events and the run length were comparable to wild-type K560GFP. However, the velocity was lower than wild type, and comparable to the value obtained in multiple motor assays. Thus, the primary single molecule motility defect in the E311A mutant is a lowered velocity of motion.

The L11 triple mutant was also motile in this assay, but motility events were more infrequent than wild type [14.6

$\pm$ 1 movements s^{-1} (μm axoneme)$^{-1}$ (nM kinesin)$^{-1}$ for wild type vs 3.3 $\pm$ 2.1 for the L11 triple mutant]. The velocity was very slow (one-fifth of wild type), which is comparable to or slower than the multiple motor data. Due to its slow velocity, run length could not be accurately determined, because the measured dissociation rate from the axoneme is comparable to the photobleaching rate. However, the lower bound determined from the data is consistent with processivity comparable to wild type. Thus, the L11 triple mutant is defective in initiating processive movement and in its velocity of movement.

The Y138A mutant exhibited no detectable motility in this single molecule assay, although it associated with the microtubule for approximately half as long as wild type. Given the velocity of 0.12 μm/s measured in multiple motor assays, we should have observed motility events longer than $\sim$0.3 μm for the subset of molecules associated for more than 3 s. Although events of this length are easily detectable, we observed none. Furthermore, vectors plotted between the attachment and detachment positions showed no directional preference, confirming the lack of observed motility. The lack of measurable motility in this assay indicates that while Y138A is capable of motion in a multiple motor assay, it exhibits little or no processive motion as a single dimer.

DISCUSSION

In the study, we have performed kinetic and single molecule analyses of kinesin alanine mutants that exhibit defects in microtubule-stimulated ATPase and microtubule gliding activities. The mutated residues are highly conserved in the kinesin superfamily, which suggests that they play important roles in the force transduction pathway. Since all of the residues examined in this study are solvent-exposed, it is unlikely that these alanine mutations produce gross conformational changes in protein structure (*39*). This notion is supported by our present findings that mantATP binds to all of the mutant K420s with similar kinetics to the wild-type motor. Thus, the mutant proteins fold into a configuration that approximates the wild-type motor, at least as far as nucleotide binding is concerned. However, subsequent steps in the enzymatic cycle (hydrolysis, product release, and possible conformational transitions) are altered in specific ways by the mutations, as discussed below.

Pre-Steady-State ATPase Kinetics. (A) Y138A and L11 Triple Are Defective in Nucleotide Hydrolysis. The Y138A and the L11 triple mutants both showed a significant decrease in the rate of nucleotide hydrolysis, as determined by manual quenching and quench-flow experiments. The defect with Y138A is particularly dramatic, as no initial burst of phosphate production was observed in the presence or absence of microtubules. Since the fluorescence signal of mantATP binding was even faster than that of wild-type K420, the rate-limiting step in the Y138A enzyme cycle is likely to be the $\beta-\gamma$-pyrophosphate bond cleavage step itself. For the L11 triple, a burst was observed, but was 50-fold slower than wild type in the absence of microtubules, and the rate was also lower in the presence of microtubules. Microtubules are still capable of stimulating the hydrolysis rates in the Y138A and L11 triple mutants, though.

Interestingly, both Y138 and the L11 triple residues (L248, D249, E250) are distant from the active site and do not interact with the β- and γ-phosphate groups or the catalytic water molecule directly. Hence, the hydrolysis effects of these mutations are likely to be indirect, most likely producing subtle changes in the active site. For example, Y138 is positioned in close proximity to the switch I loop (*21*) (Figure 1), which makes contact with the phosphates and active site magnesium. The alanine mutation may alter the conformation of switch I in a manner that impairs the hydrolysis reaction. The L11 residues are located at the tip of a disordered loop (switch II loop), which is more distant from the active site. However, a mutation of a residue at the base of the L11 loop (G234A) impairs the hydrolysis rate by >1000-fold (*31*), indicating that this loop plays a critical role in bond cleavage. The equivalent switch II loop in G proteins plays an important role in positioning the catalytic water for nucleophilic attack on the $\beta-\gamma$-pyrophosphate bond (*40, 41*). In kinesin, the triple mutations at the tip of L11 may affect hydrolysis by producing subtle alterations in the base of the loop, which in turn affects the position of the catalytic water. Interestingly, mutations in the equivalent switch II loop and subsequent helix (switch II helix) in myosin can also produce strong defects in nucleotide hydrolysis (*42*).

The above nucleotide hydrolysis mutants (as well as E311A which has a more modest 5-fold reduction in the rate of nucleotide hydrolysis) also exhibited defects in the decreasing fluorescence intensity phase after binding of mantATP. This second phase was hypothesized to be related to the ATP hydrolysis step (*32*). Our results support this conclusion, since the rates of the decreasing fluorescence phase for wild-type and mutant proteins correlate reasonably well with the phosphate burst rates measured by quench-flow method. We still, however, cannot discern whether the fluorescence change corresponds to the hydrolysis step itself or to some step that is tightly linked and faster than hydrolysis (e.g., phosphate release or a preceding protein isomerization).

(B) Reduced Microtubule-Stimulated ADP Release Rate in the L11 Triple and Y138A Mutants. In the absence of microtubules, all mutants displayed normal or slightly elevated levels of mantADP release. In the absence of microtubules, this product release step limits the ATP turnover rate (*15*). However, microtubule-stimulated release of mantADP was 2- and 4-fold slower for the L11 triple and Y138A mutants at 9 μM microtubules, respectively, and the maximal rates were slower than that of the wild type as well (see Figure 6). These results suggest that the tip of L11 and Y138A may participate in the communication pathway by which microtubules allosterically activate the product release step. Based upon cryo-electron microscopy studies, L11 may bind in the groove between two microtubule protofilaments (*30*).

(C) The Rate-Limiting Step for the E311A Mutant. The kinetic analyses of the E311A mutant revealed a normal second-order rate constant for mantATP binding, although the ATP hydrolysis was about 5-fold slower in the absence of microtubules. However, since a phosphate burst phase was clearly observed both in the presence and in the absence of microtubules, nucleotide hydrolysis cannot be a rate-limiting step that accounts for the 3-fold reduction in microtubule-stimulated ATP turnover and gliding velocity. Remarkably, the dissociation of mantADP in the presence of microtubules

was about 3 times faster than wild-type K420, and therefore this step also cannot limit the cycle time. Collectively, these results suggest that the slow step for the E311A mutant occurs after nucleotide hydrolysis but prior to ADP release. Candidates for this rate-limiting step are phosphate release or a conformational transition of the enzyme. Further work will be directed toward deciding between these possibilities.

The location of E311 is interesting with respect to a possible involvement in transmitting information from the active site to a possible force-generating element. E311 (in the α6 helix) immediately precedes the neck linker (*4*), a region which has been implicated in mechanical amplification and directional motion (*27*, *31*, *43*). We speculate that motions of α6 could affect the position and conformation of the neck linker. E311, which is a highly conserved residue, is in an intriguing position, since the side chain of this solvent-exposed residue points toward several basic residues of the base of the switch II (L11) loop. It may therefore connect a conformational change in the active site to the α6 helix, analogous to the interactions between the switch II and III regions in the α subunit of heterotrimeric G proteins (*44*). Further studies of E311 may be interesting with regard to understanding the conformational transitions that lead to force production.

Microtubule Binding Defects. For the L12 triple mutant, we observed no microtubule stimulation of mantADP dissociation in the presence or absence of ATP. This result suggests that the L12 triple mutant binds extremely poorly to microtubules, consistent with previous direct binding measurements (*25*). However, the second-order rate constant of mantATP binding, the decreasing phase of fluorescence after mantATP binding, and the rate of mantADP dissociation all appeared normal in the L12 triple mutant. Thus, these results suggest that the L12 loop plays a major role in microtubule−kinesin interactions, but not in nucleotide binding or hydrolysis. The L11 triple mutant also has an altered microtubule interaction, since it is specifically defective in initiating processive motility in the single molecule assay. This result suggests that this flexible loop may be important in the initial binding interaction with microtubules.

Comparison of Single Molecule Data with Bulk Experiments. The three mutants studied by single molecule techniques behave similarly in multiple-motor gliding assays, moving at about one-quarter the velocity of wild-type K560. However, as single motors, they behave very differently and display characteristics that could not be anticipated from the multiple motor assays. E311A moves at approximately the same speed in both multiple- and single-motor assays. However, L11 both attaches infrequently and moves more slowly as a single motor, while Y138A exhibits no detectable motility in the single molecule assay. These differences reflect the different conditions of the motility assays. In a multiple motor assay, several motors interact with a microtubule while coupled to a common mechanical substrate, the slide. This enables them to work cooperatively, and as a result, many nonprocessive motors show robust movement in multiple motor assays, while showing no motility in single molecule assays *(27, 45)*. In the single motor assay, there is the additional requirement that the two heads of the dimer coordinate their actions to ensure that one head is attached to the microtubule at all times. The run length of the motor is a direct measure of this coordination. The lack of detectable motility for the Y138A mutant indicates that this head−head coordination necessary for processive motion is disrupted. This is consistent with the severe perturbation of the ATPase kinetics in this mutant.

ACKNOWLEDGMENT

We thank Cindy Hart for assistance with molecular biology and Ryan Case for help with figure preparation.

REFERENCES

1. Hirokawa, N. (1998) *Science 279*, 519−526.
2. Liao, G., and Gundersen, G. G. (1998) *J. Biol. Chem. 273*, 9797−9803.
3. Prahlad, V., Yoon, M., Moir, R. D., Vale, R. D., and Goldman, R. D. (1998) *J. Cell Biol. 143*, 159−170.
4. Vale, R. D., and Fletterick, R. J. (1997) *Annu. Rev. Cell Dev. Biol. 12*, 745−777.
5. Yang, J. T., Saxton, W. M., Stewart, R. J., Raff, E. C., and Goldstein, L. S. (1990) *Science 249*, 42−47.
6. Ray, S., Meyhofer, E., Milligan, R. A., and Howard, J. (1993) *J. Cell Biol. 121*, 1083−1093.
7. Schnitzer, M. J., and Block, S. M. (1997) *Nature 388*, 386−390.
8. Hua, W., Young, E. C., Fleming, M. L., and Gelles, J. (1997) *Nature 388*, 390−393.
9. Lohman, T. M., Thorn, K., and Vale, R. D. (1998) *Cell 93*, 9−12.
10. Ma, Y. Z., and Taylor, E. W. (1997) *J. Biol. Chem. 272*, 717−723.
11. Ma, Y.-Z., and Taylor, E. W. (1997) *J. Biol. Chem. 272*, 724−730.
12. Moyer, M. L., Gilbert, S. P., and Johnson, K. A. (1998) *Biochemistry 37*, 800−813.
13. Gilbert, S. P., Moyer, M. L., and Johnson, K. A. (1998) *Biochemistry 37*, 792−799.
14. Ma, Y. Z., and Taylor, E. W. (1995) *Biochemistry 34*, 13242−13251.
15. Hackney, D. D. (1988) *Proc. Natl. Acad. Sci. U.S.A. 85*, 6314−6318.
16. Gilbert, S. P., Webb, M. R., Brune, M., and Johnson, K. A. (1995) *Nature 373*, 671−676.
17. Kull, F. J., Sablin, E. P., Lau, R., Fletterick, R. J., and Vale, R. D. (1996) *Nature 380*, 550−555.
18. Sack, S., Muller, J., Marx, A., Thormahlen, M., Mandelkow, E. M., Brady, S. T., and Mandelkow, E. (1997) *Biochemistry 36*, 16155−16165.
19. Kozielski, F., Sack, S., Marx, A., Thormahlen, M., Schonbrunn, E., Biou, V., Thompson, A., Mandelkow, E.-M., and Mandelkow, E. (1997) *Cell 91*, 985−994.
20. Sablin, E. P., Case, R. B., Dai, S. C., Hart, C. L., Ruby, A., Vale, R. D., and Fletterick, R. J. (1998) *Nature 395*, 813−816.
21. Sablin, E. P., Kull, F. J., Cooke, R., Vale, R. D., and Fletterick, R. J. (1996) *Nature 380*, 555−559.
22. Gulick, A. M., Song, H., Endow, S. A., and Rayment, I. (1998) *Biochemistry 37*, 1769−1777.
23. Kull, F. J., Vale, R. D., and Fletterick, R. J. (1998) *J. Muscle Res. Cell Motil. 19*, 877−886.
24. Vale, R. D. (1996) *J. Cell Biol. 135*, 291−302.
25. Woehlke, G., Ruby, A. K., Hart, C. L., Ly, B., Hom-Booher, N., and Vale, R. D. (1997) *Cell 90*, 207−216.
26. Hiratsuka, T. (1983) *Biochim. Biophys. Acta 742*, 596−508.
27. Case, R. B., Pierce, D. W., Hom-Booher, N., Hart, C. L., and Vale, R. D. (1997) *Cell 90*, 959−966.
28. Pierce, D. W., and Vale, R. D. (1998) *Methods Enzymol. 298*, 154−171.
29. Press, W. H., Teukolsky, S. A., Vetterling, W. T., and Flannery, B. P. (1992) *Numerical recipes in C*, 2nd ed., Cambridge University Press, Cambridge, U.K.
30. Sosa, H., Dias, P., Hoenger, A., Whittaker, M., Wilson-Kubalek, E., Sablin, E., Fletterick, R. J., Vale, R. D., and Milligan, R. A. (1997) *Cell 90*, 217−224.

31. Rice, S., Lin, A. W., Safer, D., Hart, C. L., Naber, N., Carragher, B. O., Cain, S. M., Pechatnikova, E., Wilson-Kubalek, E. M., Whittaker, M., Pate, E., Cooke, R., Taylor, E. W., Milligan, R. A., and Vale, R. D. (1999) *Nature 402*, 778−784.
32. Ma, Y. Z., and Taylor, E. W. (1995) *Biochemistry 34*, 13233−13241.
33. Cheng, J.-Q., Jiang, W., and Hackney, D. D. (1998) *Biochemistry 37*, 5288−5295.
34. Hackney, D. D., Malik, A. S., and Wright, K. W. (1989) *J. Biol. Chem. 264*, 15943−15948.
35. Sadhu, A., and Taylor, E. W. (1992) *J. Biol. Chem. 267*, 11352−11359.
36. Gilbert, S. P., and Johnson, K. A. (1994) *Biochemistry 33*, 1951−1960.
37. Lockhart, A., Cross, R. A., and McKillop, D. F. (1995) *FEBS Lett. 368*, 531−535.
38. Romberg, L., Pierce, D. W., and Vale, R. D. (1998) *J. Cell Biol. 140*, 1407−1416.
39. Matthews, B. W. (1996) *FASEB J. 10*, 35−41.
40. Sondek, J., Lambright, D. G., Noel, J. P., Hamm, H. E., and Sigler, P. B. (1994) *Nature 372*, 276−279.
41. Coleman, D. E., Berghuis, A. M., Lee, E., Linder, M. E., Gilman, A. G., and Sprang, S. R. (1994) *Science 265*, 1405−1412.
42. Ruppel, K. M., and Spudich, J. A. (1996) *Mol. Biol. Cell 7*, 1123−1136.
43. Case, R. B., Rice, S., Hart, C. L., Ly, B., and Vale, R. D. (2000) *Curr. Biol. 10*, 157−160.
44. Lambright, D. G., Noel, J. P., Hamm, H. E., and Sigler, P. B. (1994) *Nature 369*, 621−628.
45. Pierce, D. W., Hom-Booher, N., Otsuka, A. J., and Vale, R. D. (1999) *Biochemistry 38*, 5412−5421.

BI9928344